CHEMISTRY OF MATERIALS

ARTICLE

pubs.acs.org/cm

Synthesis and Characterization of Manganese-Rich Silicide (α-Mn_5Si_3, β-Mn_5Si_3, and β-Mn_3Si) Nanowires

Jeremy M. Higgins,[†] Ruihua Ding,[†] and Song Jin*

Department of Chemistry, University of Wisconsin—Madison, 1101 University Avenue, Madison, Wisconsin 53706, United States

Supporting Information

ABSTRACT: The Mn—Si binary phase diagram contains seven distinct equilibrium phases; however, to date, only two phases have been reported in nanowire (NW) morphology. We report the simple reaction of Mn vapor with a Si substrate in a H_2 atmosphere to lead to the formation of NW mixtures of MnSi and three new NW phases α-Mn_5Si_3, β-Mn_5Si_3, and β-Mn_3Si, with the more Mn-rich phases formed at progressively higher temperatures from 800 to 940 °C identified using electron diffraction, together with other structural characterization techniques. Furthermore, the observation of β-Mn_5Si_3 NWs having the $D8_m$ W_5Si_3 structure type, which is a structure never observed in the Mn—Si system, represents the first report of Mn_5Si_3 polymorphism. The purposeful use of excess metal species and intentional limitation of vaporous Si species during NW synthesis has led to the first synthesis of manganese-rich silicide NWs.

KEYWORDS: nanowires, magnetic nanomaterials, manganese silicides, polymorphism

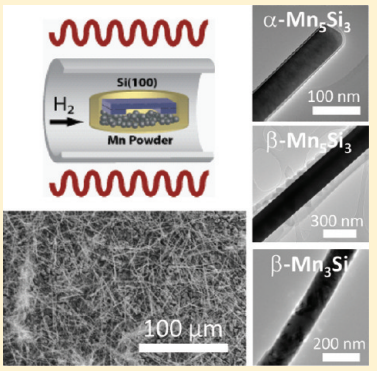

1. INTRODUCTION

Metal silicide nanowires (NWs)[1] are being investigated for a variety of technological applications, including electronics,[2−4] spintronics,[5,6] thermoelectrics,[7−9] and solar energy harvesting.[10,11] Over 20 distinct phases have been synthesized with NW morphology by the reaction of a gaseous precursor containing metal, silicon, or both, with a solid substrate, often silicon,[1] or silicidation of silicon nanowires,[12] but rational control over phase formation remains a challenge for NWs as well as bulk and thin film silicide materials.[1] While most metal—silicon systems contain multiple phases, the Mn—Si phase diagram[13] is unusually complex with seven crystallographically distinct equilibrium phases observed in bulk and thin film samples: $MnSi_{1.8}$, MnSi, Mn_5Si_3, Mn_5Si_2, Mn_3Si, Mn_4Si, and Mn_6Si (see Figure S1 in the Supporting Information). Such complexity adds to the difficulty of *a priori* prediction of silicide phase formation. The Walser—Bene "first phase rule"[14] and the effective heat of formation method,[15] both of which are based on thermodynamic and kinetic considerations, can be used to successfully predict the first phase formed in many cases, but neither works perfectly when applied to the Mn—Si system. Both rules predict that Mn_5Si_3 should form first, although the latter method also allows MnSi. Experimental observations of Mn—Si thin film diffusion couples, on the other hand, never confirm Mn_5Si_3 as the initial phase formed; rather MnSi or Mn_3Si is observed to form first.[16,17] While it is unclear what role these phenomenological rules may play in silicide NW phase formation, a thorough understanding of this NW phase formation sequence may lead to a more rigorous understanding of silicide formation in all morphologies.

NWs of the Si-rich manganese silicides, $MnSi_{1.8}$ and MnSi, have been successfully synthesized using either SSP-CVD,[8] reaction of $MnCl_2$ with Si substrates,[6,18,19] or direct conversion of silicon NWs.[20] Mn-rich silicides, similar to most metal-rich silicides, are poorly studied in bulk, as evidenced by the uncertainty in the identification of Mn_5Si_2[21] and the recent discovery of the octagonal quasicrystal $Mn_{12}Si_5$.[22] However, Mn_5Si_3 and Mn_3Si are two well-established compounds in the Mn—Si phase diagram and are both known have unusual antiferromagnetic magnetic ordering,[23−27] with Mn_3Si even suspected to be a highly unusual antiferromagnetic half-metal.[28] Various polymorphs are known to coexist in metal silicide phase diagrams, especially among phases with metal:silicon ratios of 5:3 and 3:1.[29] However, for all its other complexity the Mn—Si system has only one known Mn_5Si_3 phase, the $D8_8$ hexagonal phase, and two Mn_3Si polymorphs: a disordered cubic B2 phase (α) and a cubic $D0_3$ phase (β) (see Figure S1 in the Supporting Information).[21]

Rationally accessing new silicide NW phases still remains a challenge, but a careful analysis of published syntheses may provide insight. For example, metal-rich silicide NWs have been observed in the reactions of SiH_4 with Ni[30,31] and Ti[32] substrates, the chemical transport of metal silicide powders to Si substrates,[3,4] and the reactions of metal halides with silicon substrates[33] or silicon placed below metal or sapphire substrates.[34,35] These successful examples reveal that a rational approach to metal-rich silicide NWs should include the use of excess metal in the reaction system and/or the active limitation of vapor phase silicon precursors. Herein, we describe the simple reaction of Mn vapor with a Si substrate to synthesize NWs of Mn-rich NWs for the first time. We report the temperature-dependent phase

Received: March 14, 2011
Revised: July 7, 2011
Published: August 05, 2011

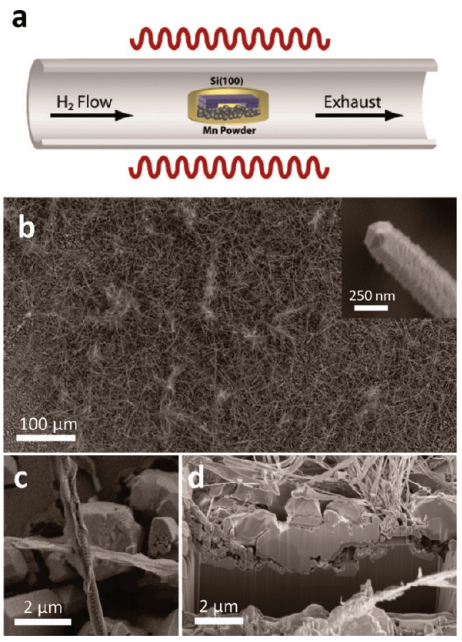

Figure 1. Synthesis scheme and SEM of as-grown substrates. (a) Diagram of the synthesis scheme illustrating the orientation of the Mn powder and Si substrates. (b) SEM micrographs show the wire density, faceted NW tips (b, inset), and (c) the NW surface structures observed in typical syntheses. (d) FIB cross-section of a growth substrate revealing an irregular film with a void space near the film/substrate interface.

formation and structural characterization of three novel Mn-rich silicide NW phases—α-Mn_5Si_3, β-Mn_5Si_3, and β-Mn_3Si. We also describe the first observation of Mn_5Si_3 polymorphism with the observation of Mn_5Si_3 NWs with either Mn_5Si_3 (α) or W_5Si_3 (β) structures.

2. EXPERIMENTAL METHODS

2.1. Synthesis of Mn-rich Silicide NWs. NW syntheses are carried out in a homemade chemical vapor deposition apparatus consisting of a tube furnace, quartz tube, and pressure and gas flow control systems. In a typical reaction, 0.2 g of Mn (99.99%, Kurt J. Lesker Company) is ground into powder and placed into an alumina boat. Three Si(100) chips coated with native oxide are cleaned for 15−20 min by sonication in deionized water, rinsed with deionized water, ethanol, and isopropanol for 5 s each, and dried with N_2. The silicon chips are placed in the boat with two chips placed directly in contact with Mn powder and suspending a larger substrate. This generates a small space between the large Si piece and the Mn powder. The system is pressurized to between 500 and 700 Torr with 140 sccm H_2 gas flow. The tube is then heated to 800−940 °C and kept for 15−60 min before cooling under vacuum.

2.2. Characterization of Silicide Growth Substrates and Individual NWs. SEM imaging and EDX spectroscopy of as-grown substrates and individual NWs were completed using a LEO 1530 SEM equipped with a SiLi X-ray detector. FIB milling of growth substrates was completed using a Zeiss 540XB CrossBeam SEM. PXRD data were collected from as-grown substrates with focused Cu Kα radiation using a Siemens STOE X-ray diffractometer and a graphite monochromator. For energy-dispersive X-ray spectroscopy (EDX) and transmission electron microscopy (TEM), the NWs are dry transferred to lacey carbon-coated copper TEM grids. A Philips CM200 TEM operated at 200 kV was used to obtain low- and high-resolution TEM images and SAED patterns from individual NWs.

3. RESULTS AND DISCUSSION

3.1. Synthesis and Characterization of Mn-rich Silicide NWs. Successful synthesis of Mn-rich silicide NWs was carried out inside of a home-built CVD reaction system described previously (Figure 1).[36] In contrast to previous manganese silicide NW syntheses,[6,8,18] we employed Mn vapor as the metal precursor to enable the delivery of Mn species to the Si growth substrate. Especially in comparison to other transition metals, Mn has a surprisingly high vapor pressure, even at the moderate temperature of 800 °C.[35,36] This precursor choice enables Mn vapor transport without significant production of gaseous Si species. The direct reaction of vaporized Mn with a suspended Si substrate in a reductive H_2 atmosphere (Figure 1a) gave rise to dense NWs growing from a crystalline film (Figure 1b) with little difference in sample morphology for reactions carried out between 800 and 940 °C from 15 min to 60 min. Typically, NWs are observed to grow in bundles nucleating from common locations on the surface. The NWs are 5−50 μm long with diameters ranging from 50 nm to 500 nm. Many are observed to have a faceted hexagonal tip (Figure 1b, inset). Notably, the NWs are all covered with a surface layer, which forms irregular fin-like structures on the NWs (Figure 1c). The size and thickness of these surface structures are quite irregular, varying considerably from wire to wire.

Many recent works have highlighted the importance of the growth substrate and various interfacial thin film on metal silicide NW synthesis.[36−38] To further analyze the growth substrate, we employed FIB milling on an 800 °C reaction substrate (Figure 1d). We observed that the NWs appear to grow from a film ∼2 μm thick. Interestingly, large voids are observed near the interface of the film with the substrate. Similar voids have been observed in films formed during the reaction of the single-source precursors $Fe(SiCl_3)_2(CO)_4$ and $CoSiCl_3(CO)_4$ over purposefully oxidized silicon substrates to produce FeSi and CoSi NWs.[38] We also note that this film appears thinnest beneath areas where NWs nucleate, perhaps indicating that Mn arriving in these areas, preferentially adding to NWs. To further analyze the products, we performed powder X-ray diffraction (PXRD) on as-grown substrates after reactions at 800, 870, and 940 °C (Figure 2a). PXRD signals are dominated by $MnSi_{1.8}$ (shown in comparison is the standard PXRD pattern of a specific phase Mn_4Si_7, which is a member of the $MnSi_{1.8}$ family[8]) and MnSi on all samples, although weak Mn_5Si_3 signals were also identified. Notably, as the reaction temperature increases, the ratio of $MnSi_{1.8}$/MnSi signal increases, indicating that $MnSi_{1.8}$ film is favored by higher reaction temperature. PXRD of such as-grown samples, which have both a thick silicide film and NWs, can be dominated by the signal from the film and may not be representative of the NW phase if the film and NWs are of different phases, as has been observed in our previous MnSi NW syntheses.[6] Definitive identification of the phase of newly synthesized NWs requires careful analysis of individual NWs.

EDX is a useful technique to characterize the elemental ratio in individual NWs and is often used to help identify a NW's phase. EDX on individual NWs (Figure 2b) shows the presence of Mn, Si, and O in the NWs themselves. The observed C, Al, and Cu signals arise from the TEM grid and Al sample holder. However, the NWs are typically covered by a large amount of irregular surface material. This surface coating can be as wide as seven times the diameter of the NW. We used EDX linescans of individual NWs to establish the elemental composition of these

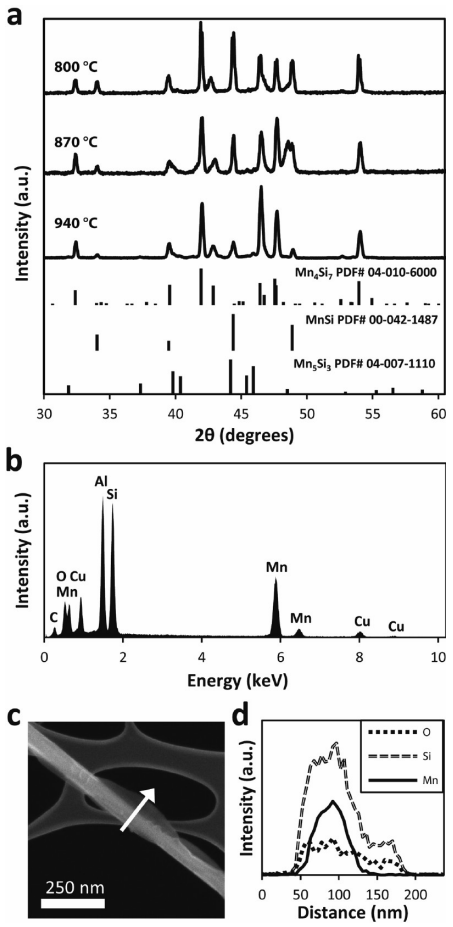

Figure 2. PXRD of as-grown substrates and EDX of NWs. (a) PXRD patterns of as-grown substrates produced at 800, 870, and 940 °C together with JCPDS standards for Mn_4Si_7, MnSi, and Mn_5Si_3. (b) EDX spectrum of a typical NW revealing the significant presence of Mn, Si, and O in individual NWs. (c) and (d) EDX line scan of a typical NW revealing the presence of Mn only in NW and Si and O in the NW and its surface structures.

surface structures (see Figures 2c and 2d). This analysis showed that this surface coating was composed entirely of Si and O with no signature of Mn observable whatsoever. Unfortunately, surface film was prevalent enough to influence EDX quantization, giving rise to overestimation of Si. Attempts to remove this surface film reproducibly without losing them from TEM grids were largely unsuccessful, as discussed further in the Supporting Information. Therefore, the utility of EDX in helping to determine the NWs composition is limited, but these measurements did provide us a lower bound of the Mn:Si ratio of roughly 1:1 (also see Figure S2 in the Supporting Information) for all NWs observed. EDX has confirmed that synthesized NWs are manganese-rich silicides different from the substrate film they grow alongside, but more careful crystallographic analysis is required to obtain more-definitive phase identification.

TEM analysis of NW samples provides rich structural information. Specifically, careful application of select area electron diffraction (SAED) and lattice resolved high-resolution TEM (HRTEM) imaging allows definitive identification of a NW crystal structure. We applied this technique to characterize the NWs synthesized at 800, 870, and 940 °C and found a very strong correlation between reaction temperature and the observed NW

Table 1. Nanowire (NW) Phases Identified by SAED

		Number of Nanowires (NWs) Identified			
reaction temperature [°C]	NWs examined	MnSi NWs	α-Mn_5Si_3 NWs	β-Mn_5Si_3 NWs	β-Mn_3Si NWs
800	20	1	19	0	0
870	17	0	16	1	0
940	21	0	1	18	2

phases. We examined at least 17 different NWs from each sample and found a mixture of phases in each case with an apparent preference for more Mn-rich phases at higher temperatures (Table 1). As we will discuss below, in addition to MnSi NWs, we found three different silicide phases—α-Mn_5Si_3, β-Mn_5Si_3, and β-Mn_3Si—that have not been observed in NW morphology until now. Further, the NWs we identify as β-Mn_5Si_3 have a structure that has not been reported in the Mn−Si binary system.

3.2. Structural Characterization of α-Mn_5Si_3 NWs. Only one Mn_5Si_3 polymorph is found in the latest Mn−Si binary phase diagram.[13] It is a hexagonal phase with the complex $D8_8$ structure type (space group $P6_3/mcm$, Pearson symbol $hP16$) for which Mn_5Si_3 is the prototype structure,[39] but we will refer to it as α-Mn_5Si_3 to avoid confusion. NWs of this phase are the most abundant in samples from 800 and 870 °C reactions and are also observed at 940 °C (Figure 3). The large diameters and thick amorphous coating can make these NWs difficult to examine using HRTEM. However, a particularly thin NW with minimal surface coating was located (Figure 3a). An HRTEM image of this NW along the α-Mn_5Si_3[101] zone axis and its fast Fourier transfer (FFT) (Figure 3b and inset) reveal plane spacings of 0.60 and 0.38 nm, in agreement (within measurement error) with the expected 0.5986 and 0.3456 nm of the (100) and (101) planes of the α-Mn_5Si_3 structure. Furthermore, we obtained multiple SAED patterns from a NW (Figure 3c−e), which can be indexed to the [110], [120], and [130] zone axes of α-Mn_5Si_3. The angles between these zone axes were measured to be [110] ∠ [120] = 31.0°, [110] ∠ [130] = 20.2°, and [120] ∠ [130] = 10.7°, similar to the expected angles between the respective pairs of Mn_5Si_3 zone axes of 30.0°, 19.1°, and 10.9°. Furthermore, the lattice parameters were calculated from the SAED patterns to be $a = 4.77 \pm 0.04$ Å and $c = 6.9 \pm 0.1$ Å and are in excellent agreement with the literature reports of $a = 4.812$ Å and $c = 6.912$ Å.[39] Careful HRTEM and SAED analysis clearly shows that these NWs are the α-Mn_5Si_3 phase, which is different from the primary phases observed in the film formed on growth substrates. This is the first report of synthesis and identification of α-Mn_5Si_3 NWs.

3.3. Structural Characterization of β-Mn_5Si_3 NWs. Interestingly, most NWs from samples synthesized at 940 °C and some NWs from 870 °C could not be identified as any reported Mn−Si phase using SAED (Figure 4). Two major structures are known among metal silicides with 5:3 metal-to-silicon stoichiometry: the Mn_5Si_3 prototype $D8_8$ structure already mentioned above and the W_5Si_3 prototype $D8_m$ structure (space group $I4/mcm$, Pearson symbol $tI32$) (Figure 4b). V_5Si_3 and Cr_5Si_3 are known to take this complex tetragonal structure; however, to our knowledge, the W_5Si_3 structure has never been reported in the Mn−Si system in bulk, thin film, or nanoscale morphologies. After careful examination and analysis of many samples, we believe that these NWs, in fact, have the tetragonal W_5Si_3 structure type, which we will call β-Mn_5Si_3. As a representative, multiple SAED

dx.doi.org/10.1021/cm2007507 |Chem. Mater. 2011, 23, 3848–3853

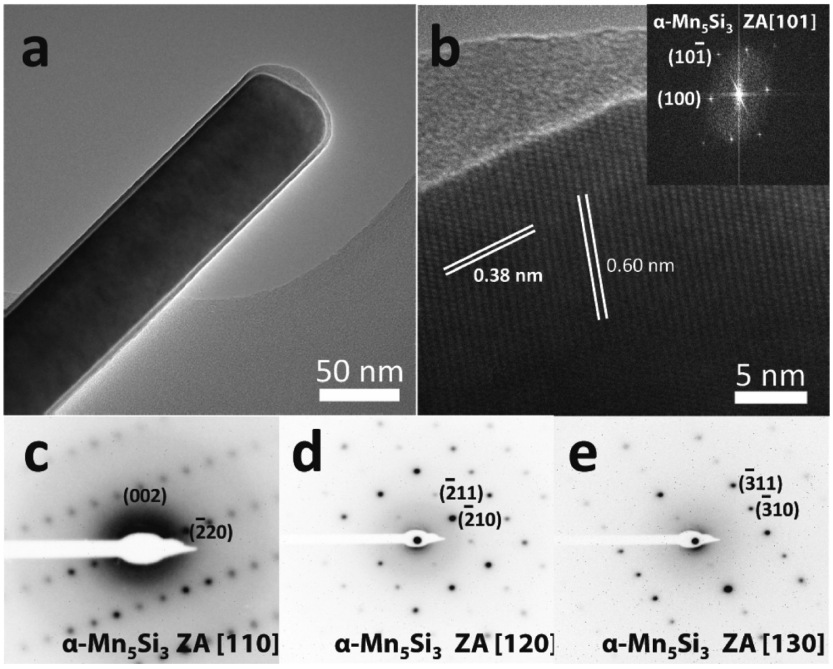

Figure 3. TEM and SAED analysis of α-Mn_5Si_3 NWs: (a) low-resolution TEM image, (b) HRTEM image, and (b, inset) indexed fast Fourier transform (FFT) of a typical NW. (c–e) Indexed SAED patterns of the α-Mn_5Si_3 along the (c) [110], (d) [120], and (e) [130] zone axes.

patterns collected from a single NW (Figure 4 c–e) can be indexed to the [110], [111], and [210] zone axes of W_5Si_3 structure, as shown by simulated diffraction patterns (Figure 4f–h). The angles between these axes were measured to be [110] ∠ [111] = 20.6°, [110] ∠ [210] = 18.7°, and [111] ∠ [210] = 27.4°, all of which agree within experimental error with the angles expected from Cr_5Si_3 (V_5Si_3), namely, 19.67° (19.62°), 18.43° (18.43°), and 26.71° (26.67°), respectively.[40,41] Furthermore, we used diffraction patterns from several NWs to calculate the lattice parameters of β-Mn_5Si_3 to be a = 9.27 ± 0.09 Å and c = 4.78 ± 0.04 Å, which are very close to the reported Cr_5Si_3 (V_5Si_3) lattice parameters a = 9.170 Å (9.420) Å and c = 4.636 Å (4.750 Å).[40,41] V, Cr, and Mn have similar metallic and covalent radii,[42] so it is not surprising that the lattice parameters of β-Mn_5Si_3 would be similar to those of the isomorphic Cr_5Si_3 and V_5Si_3. These ED analyses clearly established the existence of β-Mn_5Si_3 NWs, a novel manganese silicide phase with the W_5Si_3 structure. However, it is not clear if this newly observed "β-Mn_5Si_3" phase can only exist in nanomaterials synthesized at higher temperature or if this phase was missed in the investigation of bulk Mn–Si phase diagram.

3.4. Structural Characterization of β-Mn_3Si NWs. In reactions carried out at 940 °C, we have also sometimes observed NWs having the cubic $D0_3$ β-Mn_3Si structure (space group $Fm\bar{3}m$, Pearson symbol $cF16$) (see Figure 5).[43] SAED patterns from an example NW (Figures 5b–d) can be indexed to the [110], [210], [331] zone axes of β-Mn_3Si. The angles between these axes were measured to be [110] ∠ [210] = 18.1°, [110] ∠ [331] = 12.7°, and [210] ∠ [331] = 22.1°, similar to the expected angles of 18.44°, 13.26°, and 22.58° for the β-Mn_3Si system. Analysis of several diffraction patterns enabled the determination of the lattice parameter in β-Mn_3Si NWs to be a = 5.71 ± 0.04 Å, in excellent agreement with the literature report of a = 5.72 Å. Notably, we also observed additional spots in the [210] and [331] zone axis SAED patterns incommensurate

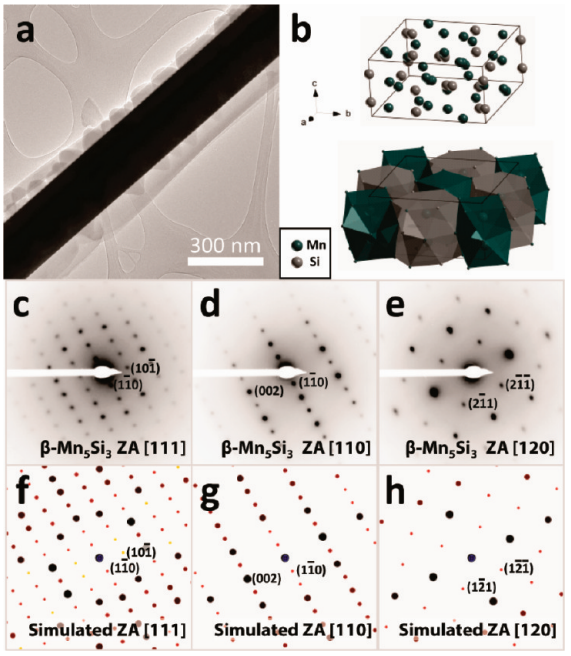

Figure 4. TEM and SAED analysis of β-Mn_5Si_3 NWs. (a) Low-resolution TEM image of a typical NW. (b) Crystal structure of β-Mn_5Si_3 having the W_5Si_3 structure type; the two views highlight the atomic positions and polyhedral stacking of the structure, respectively. (c–h) Indexed SAED patterns of the β-Mn_5Si_3 along the [111], [120], [130] zone axes are displayed above simulated patterns of the same zone axes.

with obvious expected reflections from β-Mn_3Si. The contrast observed in a low-resolution image of a typical NW (Figure 5a) indicates the presence of a high defect concentration in these NWs. Additional diffraction spots have been observed in some common NW systems, such as silicon, and recently

dx.doi.org/10.1021/cm2007507 |*Chem. Mater.* 2011, 23, 3848–3853

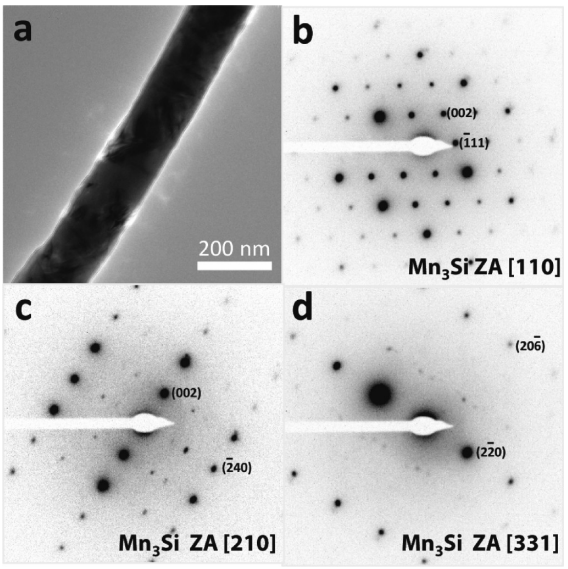

Figure 5. TEM and SAED analysis of β-Mn_3Si NWs: (a) low-resolution TEM image of a typical NW revealing much contrast from apparent defects in the crystal structure. (b–d) Indexed SAED patterns of β-Mn_3Si along the (b) [110], (c) [210], and (d) [331] zone axes. Note the additional spots in the [210] and [331] patterns.

described as being caused by nanoscale structural defects such as microtwinning.[44] DO_3 structures under stress are known to be prone to twinning,[45] but further analysis will be required to definitively correlate the structural defects with the observed unusual additional reflections.

3.5. Mn-rich Silicide NW Syntheses - Additional Observations. We attempted to obtain additional mechanistic information by varying reaction conditions, including conducting reactions at temperatures ranging from 600 °C to 940 °C. Between 600 °C and 750 °C, little deposition was observed on the Si substrates, but structures that appeared to be etch pits were observed to occur with clear crystallographic registry with the silicon substrate, likely arising from the limited formation of silane from hydrogen and silicon, a reaction that is not favorable.[46] However, between 800 and 940 °C we always observed NWs growing from a crystalline film. The only morphological difference observed when varying reaction temperature in this range was an increase in the silicide film coverage with increasing reaction temperature. These results suggest that Mn delivery is minimal below 800 °C but increases with increasing temperature, likely also giving rise to the observed temperature-dependent NW phase formation. Variation of reaction time showed that NWs grow surprisingly fast. After only 5 min of reaction at temperatures above 800 °C, NWs longer than 10 μm can be observed. There was no obvious difference in NW length after 15 min, implying that the NWs no longer grow axially after this time. However, it is observed that the amorphous surface coating on the NWs are slightly reduced for a 60-min reaction compared to the 15-min reaction, perhaps etched away by exposure to reductive atmosphere.

We also investigated how the atmosphere in the chemical vapor deposition (CVD) reactor affected NW growth. Replacing the H_2 flow gas with helium resulted in no NW growth, but we observed no effect from altering the flow of H_2 gas. Furthermore, little difference is observed in sample morphology when a H_2 pressure of 500 or 700 Torr was used, but when the reaction was completed under a 300 Torr atmosphere, only a heavy film was observed. These results suggest that the H_2 atmosphere could be crucial to initiating NW growth. However, while H_2 appears to play a role in nucleating Mn-rich NWs and enabling their anisotropic crystal growth, the exact mechanism of this process remains, as in most silicide NW syntheses, an unsolved issue.[1]

3.6. Chemical Vapor Deposition Synthesis of Manganese Silicide NWs. Comparing the published synthetic reports of manganese silicide NWs may allow us to draw some insights useful in answering the questions that still surround all silicide NW syntheses. The direct reaction of Mn metal film with a Si NW produces MnSi NWs at 650 °C,[20] a temperature lower than all other reports of manganese silicide NWs. In analogy to bulk and thin film diffusion couples,[14,15] this may indicate that MnSi is the most easily formed manganese silicide phase in NW morphology, i.e., the "first NW phase formed". In addition, two groups have reported free-standing MnSi NWs produced using the CVD reaction of vaporized $MnCl_2$ with Si substrates,[6,19] which also likely produces gaseous $SiCl_x$ species.[34] These successful syntheses required higher temperatures (875–950 °C) than the solid-state conversion reaction. Both authors believe that a careful balance of the reactions between $MnCl_2$, Si, and *in situ*-generated $SiCl_x$ are required in order to successfully produce MnSi NWs. NWs of the more Si-rich $MnSi_{1.8}$ phase have also been reported by two different groups.[8,18] We employed CVD of the single source precursor $Mn(SiCl_3)(CO)_5$ over a silicon substrate to synthesize $MnSi_{1.8}$ NWs (specifically $Mn_{19}Si_{33}$).[8] Even though the actual pyrolysis pathway for the precursor may be complicated,[38] we expect preferential delivery of Si to the growth substrate at the reported temperature (700 °C). Ham et al.[18] successfully synthesized $MnSi_{1.8}$ (specifically Mn_4Si_7) NWs through the codelivery of independent SiO and $MnCl_2$ precursors to a Si substrate at a high temperature of 1200 °C, which also likely favored the delivery of Si over Mn species to the growth substrate. It seems that the formation of a Si-rich manganese silicide phase in both syntheses was enabled by the delivery of additional Si species, but it is not currently clear whether these $MnSi_{1.8}$ NWs nucleated as this phase or if the excess Si enabled a chemical conversion from the apparently more-stable MnSi NW phase.

This article represents the first report of several Mn-rich silicide NWs. The salient feature of the current synthesis is the direct delivery of Mn vapor as the sole precursor to the silicon growth substrates. As evidenced by the lack of significant etching of Si substrates, the only Si source during growth, there should not be significant vaporous Si species present in the reaction. We believe that a combination of high Mn vapor concentration and limited gaseous Si species gave rise to these three new Mn-rich silicide NWs. The increased temperature of reaction that led to increased delivery of Mn to the substrate also gave rise to temperature-controlled phase formation. These results cannot shed light on the nucleation and growth mechanism of these new Mn-rich silicide NWs, but interestingly, the observation of MnSi NWs at lower growth temperatures does hint at the interpretation of progressive chemical conversion of NWs from MnSi to the observed Mn-rich phases with the availability of additional Mn vapor at increasingly high temperature. Much more careful analyses are underway in pursuit of further details.

4. CONCLUSION

We have reported the rational synthesis of Mn-rich silicide NWs using the direct reaction of Mn vapor with a Si substrate in a

H_2 atmosphere. NWs of MnSi, α-Mn_5Si_3, β-Mn_5Si_3, and β-Mn_3Si phases are formed progressively as the temperature is increased from 800 °C to 940 °C. This is the first observation of NWs of α-Mn_5Si_3, β-Mn_5Si_3, and α-Mn_3Si phases and, furthermore, the first observation of polymorphism in Mn_5Si_3. The clear phase formation sequence observed appears to be dependent strongly on the saturation of Mn in the atmosphere of this reaction system, an insight which has led to a better understanding of phase formation behavior in all reported manganese silicide NW syntheses.

■ ASSOCIATED CONTENT

Supporting Information. Mn−Si binary phase diagram and EDX characterization of Mn-rich silicide nanowires (NWs). This material is available free of charge via the Internet at http://pubs.acs.org.

■ AUTHOR INFORMATION

Corresponding Author

*E-mail: jin@chem.wisc.edu. URL: http://jin.chem.wisc.edu.

Author Contributions

†These authors contributed equally to this work.

■ ACKNOWLEDGMENT

We thank the NSF (CBET-1048625), University of Wisconsin−Madison Graduate School, the Sloan Research Fellowship, and Research Corporation Cottrell Scholar Award for support. R.D. also acknowledges the Hilldale Research Fellowship for support.

■ REFERENCES

(1) Schmitt, A. L.; Higgins, J. M.; Szczech, J. R.; Jin, S. *J. Mater. Chem.* **2010**, *20*, 223.
(2) Liao, L.; Lin, Y.-C.; Bao, M.; Cheng, R.; Bai, J.; Liu, Y.; Qu, Y.; Wang, K. L.; Huang, Y.; Duan, X. *Nature* **2010**, *467*, 305.
(3) Song, Y.; Jin, S. *Appl. Phys. Lett.* **2007**, *90*, 173122/1.
(4) Song, Y.; Schmitt, A. L.; Jin, S. *Nano Lett.* **2007**, *7*, 965.
(5) Schmitt, A. L.; Higgins, J. M.; Jin, S. *Nano Lett.* **2008**, *8*, 810.
(6) Higgins, J. M.; Ding, R.; De Grave, J. P.; Jin, S. *Nano Lett.* **2010**, *10*, 1605.
(7) Zhou, F.; Szczech, J.; Pettes, M. T.; Moore, A. L.; Jin, S.; Shi, L. *Nano Lett.* **2007**, *7*, 1649.
(8) Higgins, J. M.; Schmitt, A. L.; Guzei, I. A.; Jin, S. *J. Am. Chem. Soc.* **2008**, *130*, 16086.
(9) Szczech, J. R.; Schmitt, A. L.; Bierman, M. J.; Jin, S. *Chem. Mater.* **2007**, *19*, 3238.
(10) Lin, Y.; Zhou, S.; Liu, X.; Sheehan, S.; Wang, D. *J. Am. Chem. Soc.* **2009**, *131*, 2772.
(11) Lin, Y.; Zhou, S.; Sheehan, S. W.; Wang, D. *J. Am. Chem. Soc.* **2011**, *133*, 2398.
(12) Chou, Y.-C.; Lu, K.-C.; Tu, K. N. *Mater. Sci. Eng., R* **2010**, *70*, 112.
(13) Gokhale, A. B. Mn-Si Phase Diagram (1990 Gokhale A.B.). In *ASM Alloy Phase Diagrams Center*; Villars, P., Ed.; ASM International: Materials Park, OH, 2011.
(14) Walser, R. M.; Bene, R. W. *Appl. Phys. Lett.* **1976**, *28*, 624.
(15) Pretorius, R. *Mater. Res. Soc. Symp. Proc.* **1984**, *25*, 15.
(16) Eizenberg, M.; Tu, K. N. *J. Appl. Phys.* **1982**, *53*, 6885.
(17) Zhang, L.; Ivey, D. G. *J. Mater. Res.* **1991**, *6*, 1518.
(18) Ham, M.-H.; Lee, J.-W.; Moon, K.-J.; Choi, J.-H.; Myoung, J.-M. *J. Phys. Chem. C* **2009**, *113*, 8143.
(19) Seo, K.; Yoon, H.; Ryu, S.-W.; Lee, S.; Jo, Y.; Jung, M.-H.; Kim, J.; Choi, Y.-K.; Kim, B. *ACS Nano* **2010**, *4*, 2569.
(20) Lin, Y.-C.; Chen, Y.; Shailos, A.; Huang, Y. *Nano Lett.* **2010**, *10*, 2281.
(21) Gokhale, A. B.; Abbaschian, R. *Bull. Alloy Phase Diagrams* **1990**, *11*, 468.
(22) Cao, W.; Ye, H. Q.; Kuo, K. H. *Phys. Status Solidi A* **1988**, *107*, 511.
(23) Tomiyoshi, S.; Watanabe, H. *J. Phys. Soc. Jpn.* **1975**, *39*, 295.
(24) Tomiyoshi, S.; Cowley, E. R.; Onodera, H. *Phys. Rev. B* **2006**, *73*, 024416/1.
(25) Menshikov, A. Z.; Vokhmyanin, A. P.; Dorofeev, Y. A. *Phys. Status Solidi B* **1990**, *158*, 319.
(26) Brown, P. J.; Forsyth, J. B. *J. Phys.: Condens. Matter* **1995**, *7*, 7619.
(27) Silva, M. R.; Brown, P. J.; Forsyth, J. B. *J. Phys.: Condens. Matter* **2002**, *14*, 8707.
(28) Pfleiderer, C. *Phys. B* **2003**, *329−333*, 1085.
(29) Maex, K.; Van Rossum, M.; Reader, A. Crystal Structure of TM Silicides. In *Properties of Metal Silicides*; Maex, K., Van Rossum, M., Eds.; INSPEC, the Institution of Electrical Engineers: London, U.K., 1995; pp 3.
(30) Kang, K.; Kim, C.-J.; Jo, M.-H. *J. Appl. Phys.* **2009**, *105*, 122407/1.
(31) Kim, C.-J. K.; Kibum; Woo, Y. S.; Ryu, K.-G.; Moon, H.; Kim, J.-M.; Zang, D.-S.; Jo, M.-H. *Adv. Mater.* **2007**, *19*, 3637.
(32) Chang, C.-M.; Chang, Y.-C.; Lee, C.-Y.; Yeh, P.-H.; Lee, W.-F.; Chen, L.-J. *J. Phys. Chem. C* **2009**, *113*, 9153.
(33) Lin, H.-K.; Tzeng, Y.-F.; Wang, C.-H.; Tai, N.-H.; Lin, I. N.; Lee, C.-Y.; Chiu, H.-T. *Chem. Mater.* **2008**, *20*, 2429.
(34) Varadwaj, K. S. K.; Seo, K.; In, J.; Mohanty, P.; Park, J.; Kim, B. *J. Am. Chem. Soc.* **2007**, *129*, 8594.
(35) In, J.; Seo, K.; Lee, S.; Yoon, H.; Park, J.; Lee, G.; Kim, B. *J. Phys. Chem. C* **2009**, *113*, 12996.
(36) Schmitt, A. L.; Bierman, M. J.; Schmeisser, D.; Himpsel, F. J.; Jin, S. *Nano Lett.* **2006**, *6*, 1617.
(37) Kang, K.; Kim, S.-K.; Kim, C.-J.; Jo, M.-H. *Nano Lett.* **2008**, *8*, 431.
(38) Higgins, J. M.; Carmichael, P.; Schmitt, A. L.; DeGrave, J. P.; Lee, S.; Jin, S. *ACS Nano 5*, 3268−3277 (DOI: 10.1021/nn200387y).
(39) Lander, G. H.; Brown, P. J. *Philos. Mag.* **1967**, *16*, 521.
(40) Dauben, C. H.; Templeton, D. H.; Myers, C. *J. Phys. Chem.* **1956**, *60*, 443.
(41) Rawn, C. J.; Schneibel, J. H.; Fu, C. L. *Acta Mater.* **2005**, *53*, 2431.
(42) In *CRC Handbook of Chemistry and Physics*, 91st ed.; Haynes, W. M., Ed.; CRC Press: Boca Raton, FL, 2010.
(43) Babanova, E. N.; Sidorenk, Fa; Geld, P. V.; Basov, N. I. *Fiz. Met. Metalloved.* **1974**, *38*, 586.
(44) Cayron, C.; Den Hertog, M.; Latu-Romain, L.; Mouchet, C.; Secouard, C.; Rouviere, J.-L.; Rouviere, E.; Simonato, J.-P. *J. Appl. Crystallogr.* **2009**, *42*, 242.
(45) Park, K. T.; Goo, E. *Acta Metall. Mater.* **1991**, *39*, 3027.
(46) Jasinski, J. M.; Gates, S. M. *Acc. Chem. Res.* **1991**, *24*, 9.